Nigerian Journal of Theoretical and Environmental Physics (NJTEP)
ISSN Print: 3026-9601
ISSN Online: 1597-9849
DOI: https://doi.org/10.62292/njtep.v4i2.2026.122
Volume 4(2), June 2026

Structural, Electronic, Elastic and Mechanical Properties of NaMgZ (Z = P, As, Sb): Implications for Thermoelectric Applications

***[1,2]Solomon T. Tonga, [2]Jamu B. Yerima, [2]Abubakar D. Ahmed and [3]Abdulrafiu T. Raji**

[1]Taraba State University, Jalingo, Taraba State, Nigeria.
[2]Modibbo Adama University, Yola, Adamawa State, Nigeria.
[3]The Deanery, University of South Africa, Science Campus, Corner of Christiaan de Wet Road and Pioneer Avenue, Florida, 1709, South Africa.

[*]Corresponding author's email: ahiru.tonga@tsuniversity.ng

ABSTRACT

Half-Heusler semiconductors remain attractive thermoelectric materials because their electronic structure, mechanical stability, and transport response can be tuned efficiently through chemical substitution. In this work, we investigate the NaMgZ (Z = P, As, Sb) series using first-principles density functional theory (DFT) within the generalized gradient approximation of Perdew-Burke-Ernzerhof (GGA-PBE), as implemented in Quantum ESPRESSO, in order to clarify how progressive pnictogen substitution modifies structural stability, band-gap magnitude, elastic behavior, and the thermoelectric descriptors that emerge from these quantities. All three compounds are found to be mechanically stable in the cubic half-Heusler phase, with the equilibrium lattice constant increasing systematically from 6.36 Å (NaMgP) to 6.91 Å (NaMgSb) and the computed band gap narrowing from 1.46 eV in NaMgP to 0.88 eV in NaMgAs before rising again to 1.20 eV in NaMgSb, reflecting a non-monotonic but chemically tunable route for band-gap engineering through composition. Negative formation energies confirm thermodynamic stability across the series, while the elastic constants, bulk modulus, shear modulus, Young's modulus, and Debye temperature reveal progressive mechanical softening from the lighter to the heavier members. All three compounds retain clear semiconducting character across the studied range, with the intermediate gaps of NaMgAs and NaMgSb supporting a favorable balance between carrier activation and Seebeck response. Taken together, these results identify the NaMgZ family as a chemically tunable platform in which the balance between electrical transport and lattice dynamics can be optimized for thermoelectric applications, with NaMgAs and NaMgSb emerging as the most promising candidates for a favorable compromise between band gap, carrier mobility, and lattice thermal transport.

Keywords:
NaMgSb,
Band Gap,
Half-Heusler Compounds,
Density Functional Theory.

INTRODUCTION

Thermoelectric energy conversion has become an important research direction because it offers a direct route for transforming waste heat into useful electrical power and, conversely, for achieving compact solid-state refrigeration. The efficiency of a thermoelectric material is commonly quantified by the dimensionless figure of merit $ZT = S^2\sigma T/\kappa$, where S denotes the Seebeck coefficient, σ is the electrical conductivity, T is the absolute temperature, and κ is the total thermal conductivity. Achieving a high ZT is intrinsically difficult because these transport coefficients are strongly coupled: increasing carrier concentration may improve electrical conductivity but often lowers the Seebeck coefficient, while the reduction of thermal conductivity should ideally be achieved without degrading electronic transport. As a result, modern thermoelectric materials research has focused on compounds in which the electronic structure and lattice dynamics can be tuned in a chemically controlled manner (Zhao et al., 2017; Huang et al., 2016). More recent reviews have reinforced this picture, emphasizing that translating half-Heusler power-factor gains into device-level performance requires the simultaneous engineering of band convergence, valley

degeneracy, and phonon scattering channels (Quinn & Bos, 2021; Miao et al., 2024).

Within this broader context, half-Heusler compounds have emerged as one of the most versatile classes of thermoelectric materials. Their appeal lies in a favorable combination of phase stability, semiconducting electronic structure, moderate to high carrier mobility, and extensive compositional flexibility. In many half-Heusler systems, the valence and conduction bands can be adjusted through selective substitution on one or more sublattices, thereby enabling control over the band gap, band dispersion, carrier effective mass, and phonon response. Such tunability is particularly valuable for thermoelectric design because an ideal composition should possess a sufficiently large gap to suppress bipolar conduction while retaining enough band dispersion to sustain useful electrical conductivity. At the same time, relatively soft lattice dynamics and low characteristic phonon frequencies are often desirable for reducing the lattice contribution to thermal conductivity (Jaishi et al., 2021; Chen et al., 2018; Huang et al., 2016).

The NaMgZ (Z = P, As, Sb) family provides an excellent model system for exploring these competing requirements. The series preserves the same basic crystal chemistry while systematically varying the pnictogen atom from a light to a heavy element. This strategy allows the effect of chemical substitution to be examined with minimal structural ambiguity. As the pnictogen changes from P to Sb, one expects a progressive increase in atomic size, stronger relativistic effects, modified *p*-orbital participation near the band edges, and weakened average bonding. These changes can lead to simultaneous variation in equilibrium lattice constant, elastic stiffness, Debye temperature, band-gap magnitude, and ultimately the transport balance that determines thermoelectric usefulness. Because the compounds are chemically related, the NaMgZ series is especially well suited for identifying robust composition–property trends rather than isolated single-composition observations.

An additional motivation for studying NaMgZ arises from its inherent structural and bonding characteristics. The presence of sodium tends to produce a relatively expanded lattice and a weaker average bonding environment, which can significantly influence both the electronic and vibrational subsystems. In practical terms, these features may modify the curvature of the frontier electronic bands, alter the intrinsic carrier activation energy, and promote lattice softening. Such effects directly impact the balance among electrical conductivity, Seebeck coefficient, and lattice thermal conductivity. Understanding these interrelated factors is important for identifying how compositional tuning can be employed as a rational strategy to optimize thermoelectric performance in half-Heusler-derived compounds (Idrissi et al., 2023; Anuradha et al., 2018; Yadav & Sanyal, 2015). While Li-based half-Heusler analogues such as LiMgZ have received comparatively detailed first-principles attention (Idrissi et al., 2023; Parsamehr et al., 2021), the corresponding Na-based series remains far less explored, despite the fact that the larger ionic radius and weaker electronegativity of Na relative to Li are expected to produce a more expanded lattice, softer elastic response, and potentially more favorable phonon scattering for thermoelectric purposes. This relative scarcity of systematic, chemically resolved first-principles data for Na-based half-Heuslers is the specific gap that the present NaMgZ study addresses.

The aim of the present work is therefore to provide a systematic first-principles study of NaMgP, NaMgAs and NaMgSb with emphasis on band-gap engineering and its consequences for thermoelectric applications. Specifically, we evaluate the convergence behavior of the computational parameters, determine the optimized crystal structures, assess thermodynamic and mechanical stability through formation energies and elastic constants, and analyze the evolution of the electronic structure across the series. Particular attention is paid to how the band gap narrows from the lighter to the heavier pnictogen compounds and how this narrowing is accompanied by progressive elastic softening and lower Debye temperature. These trends are then discussed in the framework of thermoelectric materials design, where the best composition is expected to balance semiconducting behavior, adequate carrier mobility, and reduced phonon-mediated heat transport.

By organizing the discussion around a chemically coherent material family, this study seeks to establish a clear structure–property–function relationship for NaMgZ compounds. The results not only clarify the influence of pnictogen substitution on structural, electronic, and mechanical behavior, but also identify the compositions that are most promising for further transport calculations, doping strategies, and experimental verification. In this sense, the present work is intended to contribute both a materials-specific analysis of NaMgZ and a broader demonstration of how band-gap engineering can be used to guide the search for improved thermoelectric half-Heusler systems.

MATERIALS AND METHODS

Computational Details

The structural, electronic, and mechanical properties of NaMgZ (Z = P, As, Sb) were investigated using first-principles density functional theory as implemented in the QuantumESPRESSO package (Giannozzi et al., 2020; Giannozzi et al., 2017). The exchange–correlation effects were described within the generalized gradient approximation using the Perdew–Burke–Ernzerhof (GGAPBE) functional (Perdew et al., 1996). Projector augmented-wave (PAW) pseudopotentials were employed throughout, generated within the framework of

Blöchl (1994). Standard scalar-relativistic PAW pseudopotentials were used for Na, Mg, P and As and a fully relativistic PAW pseudopotential including spin-orbit coupling was used for Sb, generated within the PSlibrary distribution for Quantum ESPRESSO (version 7.1). Neither a semi-empirical van der Waals dispersion correction (e.g., DFT-D2/D3) nor a Hubbard U correction was applied in this work: the NaMgZ compounds contain no van der Waals-bonded layered motifs and no partially filled d or f shells that would be expected to require an on-site Hubbard correction, so standard GGA-PBE is considered adequate for the structural, elastic, and electronic properties reported here. Electronic band structures were computed along high-symmetry path of the face-centred-cubic Brillouin zone, W-L-Gamma-X-W-K, using Gaussian smearing with a width of 0.01 Ry for self-consistent-field calculations; the projected density of states (PDOS) was obtained on the same relaxed structures using a denser non-self-consistent k-mesh. Post-processing and visualization of the band structures, PDOS, and elastic-constant results were performed using in-house Python scripts built on the Atomic Simulation Environment (ASE) and Matplotlib.

A Monkhorst–Pack *k*-point mesh of 15×15×15 was used for Brillouin-zone sampling (Monkhorst & Pack, 1976), while the plane-wave cutoff energy was set to 150 Ry for the production calculations. These parameters were selected after systematic convergence tests with respect to *k*-point density, cutoff energy, and lattice parameter, so that the total energy was numerically stable within the adopted convergence tolerance. Full structural relaxation was performed for each compound prior to the calculation of electronic and mechanical properties, allowing both the lattice parameters and internal atomic positions to reach their optimized equilibrium values. Because relativistic effects are expected to be strongest for the Sb-containing compound, spin–orbit coupling (SOC) was explicitly included in the NaMgSb calculations.

After structural optimization, the equilibrium geometries were used to compute the electronic band structures and related ground-state properties. For this work, the mechanical response was computed using the Thermo_PW module interfaced with quantum espresso and for a cubic crystal, it is fully described by the three independent elastic constants C_{11}, C_{12}, and C_{44}, where C_{11} measures the resistance to longitudinal strain, C_{12} represents the coupling between orthogonal normal strains, and C_{44} characterizes resistance to shear deformation (Rogl et al., 2016; Husain et al., 2023, Dal Corso 2016). The bulk modulus was obtained from

$$B = \frac{C_{11}+2C_{12}}{3} \quad (1)$$

To evaluate the isotropic polycrystalline response, the Voigt and Reuss shear moduli were calculated as

$$G_V = \frac{C_{11}-C_{12}+3C_{44}}{5},\ G_R = \frac{5(C_{11}-C_{12})C_{44}}{4C_{44}+3(C_{11}-C_{12})} \quad (2)$$

And the Hill average,

$$G = \frac{G_V+G_R}{2} \quad (3)$$

Was used as the effective shear modulus. Young's modulus and Poisson's ratio were then determined from

$$E = \frac{9BG}{3B+G},\ \nu = \frac{3B-2G}{2(3B+G)} \quad (4)$$

Mechanical stability was assessed using the born criteria for cubic crystals,

$$C_{11}-C_{12} > 0,\ C_{11}+2C_{12} > 0,\quad 3C_{44} > 0 \quad (5)$$

The formation energy per atom was calculated according to

$$E_f = \frac{E_{tot}(NaMgZ)-\mu Na-\mu Mg-\mu Z}{3} \quad (6)$$

Where E_{tot} (NaMgZ) is the total energy of the compound and μ_i denotes the reference chemical potential of each elemental constituent in its stable phase. This expression was used to assess the thermodynamic stability of the NaMgZ series with respect to the elemental reference states.

Data Sources

Meteorological data including temperature and relative humidity—were retrieved from NASA's Atmospheric Infrared Sounder (AIRS) onboard the EOS Aqua satellite. The dataset used corresponds to Level 3 daily gridded observations, covering pressure levels of 1000 hPa, 850 hPa, and 600 hPa at a spatial resolution of 1° × 1°, for the years 2003 and 2024.

Geomagnetic activity was quantified using the hourly Disturbance Storm Time (Dst) index, obtained from the World Data Center for Geomagnetism. The Dst index serves as a global measure of the intensity of geomagnetic storms, reflecting the strength of the symmetric ring current in the magnetosphere.

RESULTS AND DISCUSSION

In this study, the NaMgZ (Z = P, As, Sb) half-Heusler compounds are explored to better understand their structural, electronic, elastic, and mechanical properties, with the goal of assessing how well they can be tuned for thermoelectric applications. The inclusion of sodium tends to expand the lattice slightly and alters the bonding environment, which can have noticeable effects on the material's stability, electronic structure, and mechanical behavior. By examining properties such as lattice parameters, band structure, elastic constants, and related mechanical indicators, it becomes possible to build a

clearer picture of how these materials respond to stress and how stable they are under different conditions. This information is important for evaluating their durability and overall suitability for use in thermoelectric devices. Figures 1–5 illustrate the convergence tests, optimized structures, and key electronic features of the NaMgZ compounds.

Convergence of Computational Parameters

Accurate density-functional-theory calculations require well-defined convergence of numerical settings. For each NaMgZ compound, systematic tests were performed for (i) k-point density, (ii) plane-wave cutoff energy, and (iii) equilibrium lattice constants. The convergence threshold was a total-energy variation below 1m Ry per atom.

K-point Convergence

Figure 1 shows how the total energy of the NaMgZ compounds evolves with increasing k-point density during Brillouin-zone sampling. For all compositions, the total energy decreases steadily as the k-point mesh becomes denser and begins to stabilize from a k-point grid of about 5, beyond which further increases produce only negligible changes. This behavior clearly indicates that convergence is effectively achieved starting from this point. The smooth trend also reflects the numerical stability of the calculations and confirms that the electronic states across the Brillouin zone are being sampled with sufficient accuracy.

Achieving reliable convergence requires the use of relatively dense k-point meshes, which is related to the larger lattice dimensions of these compounds. The expanded lattice reduces the size of the reciprocal space, making the system more sensitive to k-point sampling. Consequently, a finer grid is needed to accurately capture important features of the electronic structure, particularly near band extrema. The absence of irregular fluctuations or discontinuities further supports the reliability of the results and indicates that the calculations are free from numerical artifacts (Arif et al; 2016).

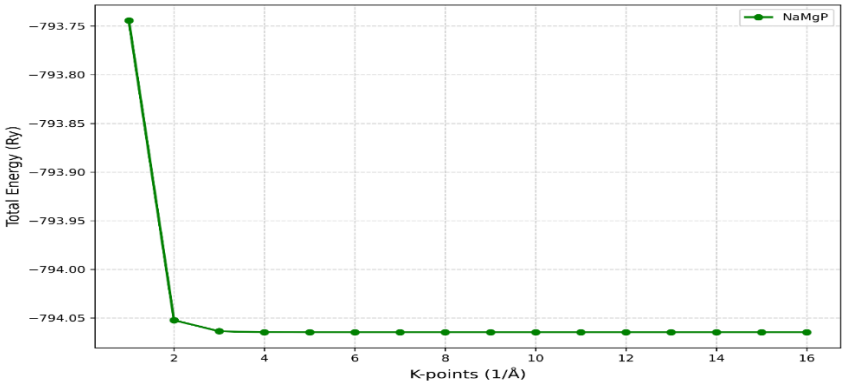

(a) NaMgP

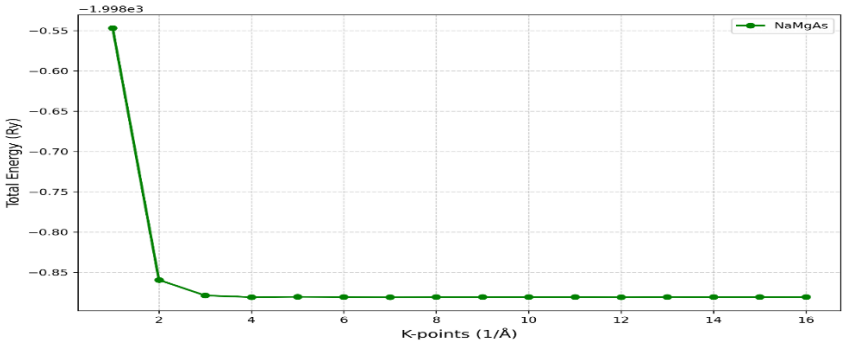

(b) NaMgAs

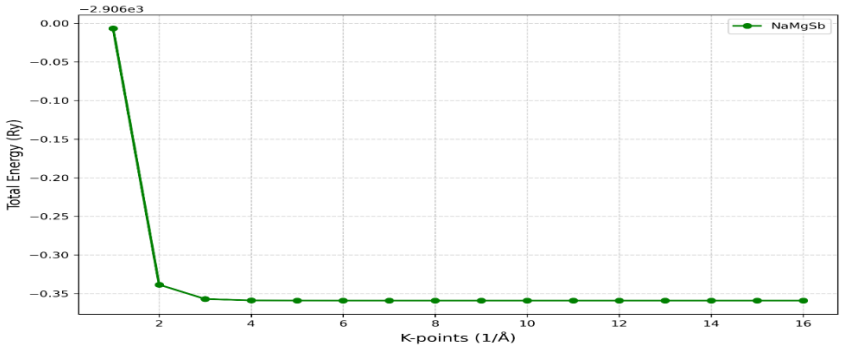

(c) NaMgSb

Figure 1: K-point convergence tests for NaMgZ (Z = P, As, Sb) showing a convergence at 4 per angstrom

Cutoff-Energy Convergence

The plane-wave cutoff energy convergence results shown in Figure 2 reveal a smooth and steady stabilization of the total energy as the cutoff energy increases. For all NaMgZ compounds, the total energy gradually decreases and becomes stable from around 50 Ry, beyond which further increases lead to only very small changes. This shows that convergence is effectively achieved from this point. However it should be noted that, for accuracy sake, this work utilizes 150 Ry as noted in the previous section The absence of any irregular behavior in the curve indicates that the calculations are well-behaved and reliable. Reaching convergence at this cutoff ensures that the results obtained for the structural, electronic, and mechanical properties are accurate and consistent.

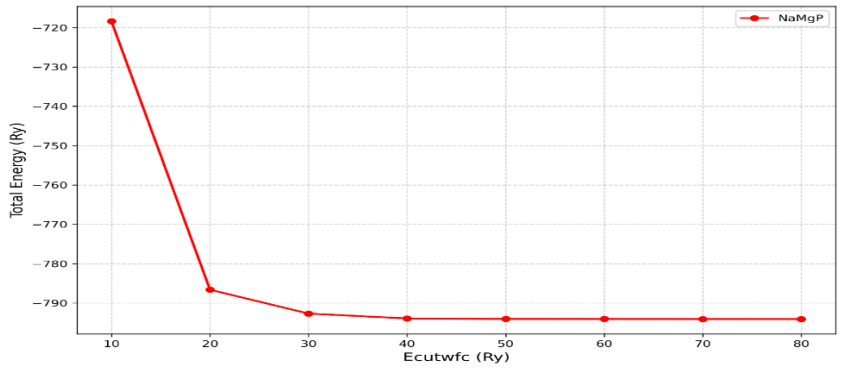

(a) NaMgP

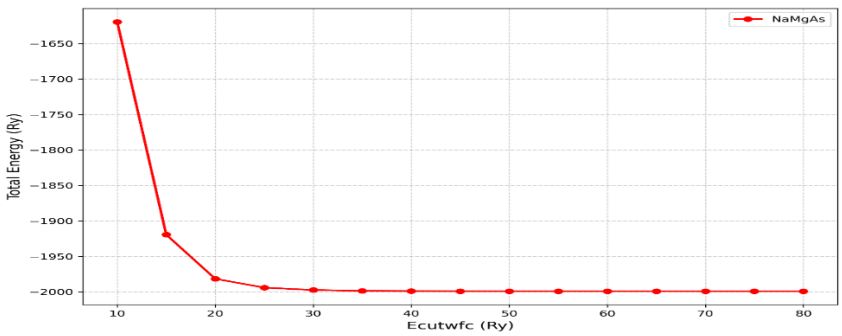

(b) NaMgAs

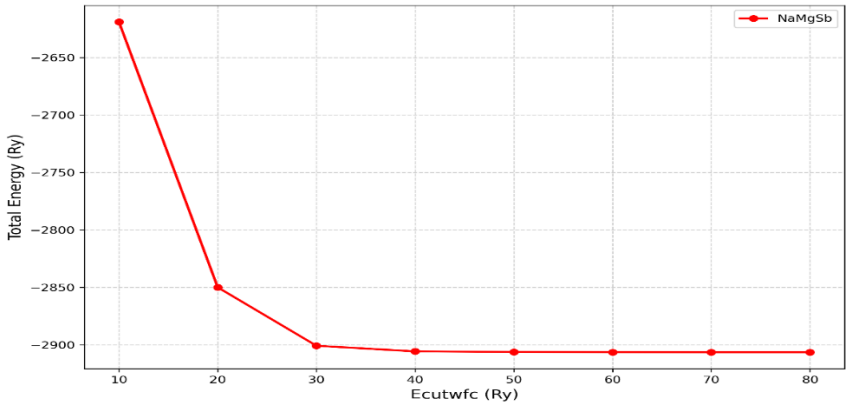

(c) NaMgSb

Figure 2: Cutoff-energy convergence for NaMgZ (Z = P, As, Sb) showing convergence at 50 Ry

Lattice-Parameter Convergence

Figure 3 illustrates the variation of total energy with lattice parameter for the NaMgZ compounds. Each curve shows a clear and well-defined minimum, confirming that all compositions possess a stable equilibrium structure. The smooth shape of the curves around these minima further indicates that the structures are mechanically stable within the studied range.

The calculated equilibrium lattice constants show a consistent increase from NaMgP to NaMgSb reflecting the expected trend based on atomic size. Importantly, these results are in excellent agreement with previously reported values in the literature (Arif et al; 2016), as summarized in Table 1, which further validates the accuracy and reliability of the present calculations.

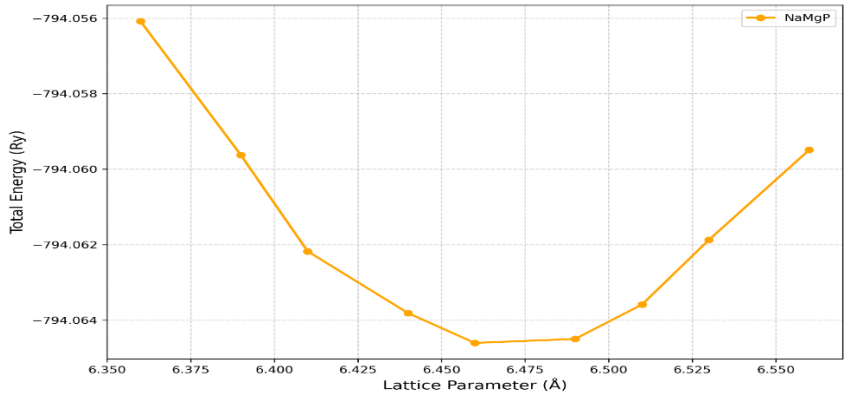

(a) NaMgP

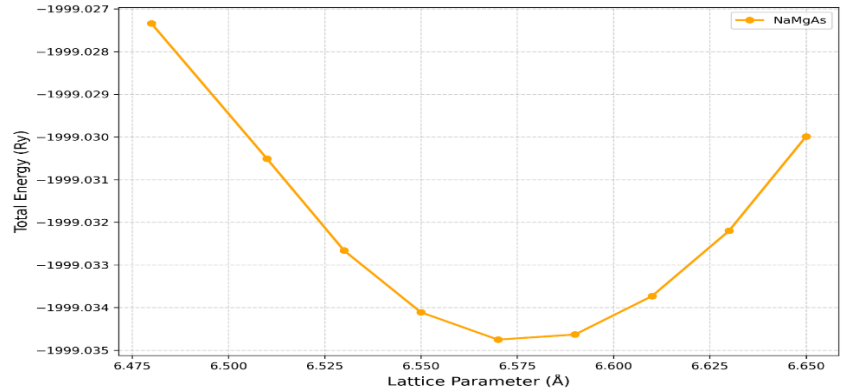

(b) NaMgAs

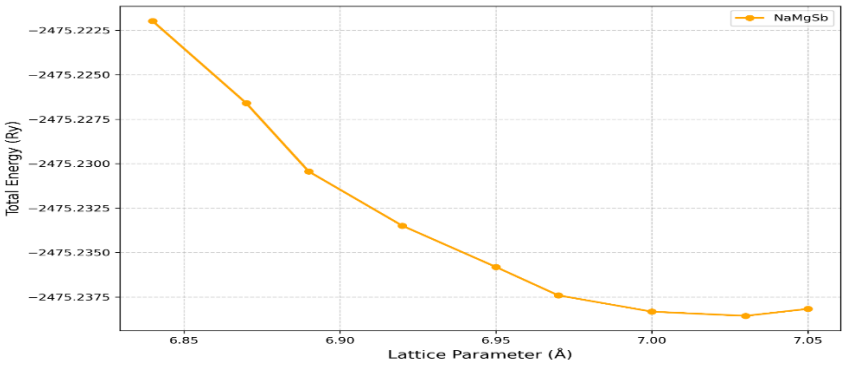

(c) NaMgSb

Figure 3: lattice parameter convergence tests for NaMgZ compounds: (a) NaMgP, (b) NaMgAs and (c) NaMgSb

Optimized Crystal Structures

Figure 4 shows the relaxed crystal structures of the NaMgZ compounds. All compositions maintain the cubic half-Heusler structure with space group $F\bar{4}3m$ after full optimization. There is no sign of symmetry breaking or structural distortion, and all atoms remain close to their ideal positions, showing that the structures are stable and well-balanced.

This structural stability is important for thermoelectric applications, where materials are expected to perform reliably under thermal stress. The preserved cubic symmetry also supports uniform (isotropic) transport properties, which is beneficial for device performance.

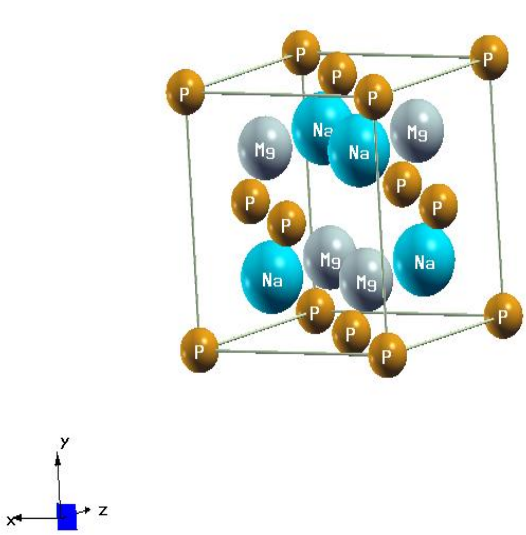

(a) NaMgP

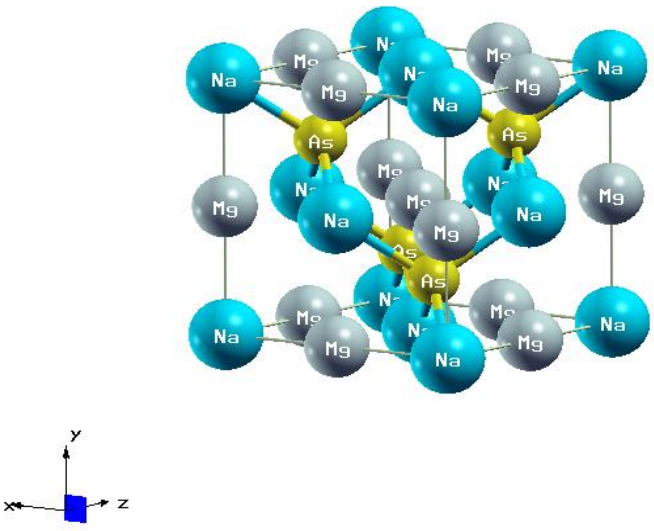

(b) NaMgAs

(c) NaMgSb

Figure 4: Relaxed crystal structures of NaMgZ (Z = P, As, Sb)

Lattice Constants, Band Gaps, and Formation Energies

The results in Table 1 show clear trends in the NaMgZ compounds. The lattice constant increases steadily from NaMgP to NaMgSb, mainly due to the larger size because atomic radius increase from P to Sb . The band gap decreases across the series, which suggests easier carrier excitation at higher temperatures which is an advantage for thermoelectric performance. These values are consistent with previously reported studies, with only small differences due to computational methods (Arif et al; 2016).

All compounds have negative formation energies, which confirms that they are thermodynamically stable and unlikely to decompose into their elemental forms. In simple terms, this means the materials can exist stably in practice. The results suggest that NaMgZ compounds are structurally stable, electronically tunable, and suitable for thermoelectric applications.

Table 1: Lattice Constants, Band Gaps, and Formation Energies of Namgz Compounds. Superscripts Indicate Literature References For Lattice Constants and Band Gaps

Compound	a (Å, this work)	a (Å, lit.)	E_g (eV, this work)	E_g (eV, lit.)	E_f (eV/atom)
NaMgP	6.36	6.33[a]	1.46	1.47[a]	-0.252
NaMgAs	6.55	6.50[a]	0.88	0.83[a]	-0.758
NaMgSb	6.91	6.92[a]	1.20	1.87[a]	-0.651

[a] Arif et al., 2016.

Elastic Constants and Mechanical Properties

The elastic behavior of NaMgZ compounds is governed by the three independent elastic constants of the cubic phase. In this framework, C_{11} describes resistance to uniaxial compression along the principal crystallographic directions, C_{12} measures the elastic coupling between perpendicular normal strains, and C_{44} represents the resistance to shear distortion. For mechanical stability, a cubic crystal must satisfy the Born conditions $C_{11} - C_{12} > 0$, $C_{11} + 2C_{12} > 0$, and $C_{44} > 0$ (Born 1940). All NaMgZ compounds satisfy these requirements, confirming that the optimized half-Heusler structures are mechanically stable (Rogl et al., 2016, Born 1940).

The corresponding polycrystalline elastic parameters provide a compact physical summary of the mechanical response. The bulk modulus B quantifies resistance to uniform volume change, the shear modulus G measures resistance to shape deformation, Young's modulus E reflects the overall axial stiffness, and Poisson's ratio v describes the lateral strain induced by uniaxial loading. The values listed in Table 2 were obtained from the Voigt–Reuss–Hill averaging scheme described in the computational details

Within the NaMgZ series, the progressive decrease of C_{11} and C_{44} from NaMgP to NaMgSb shows that both the longitudinal and shear rigidity weaken as the pnictogen becomes heavier. The comparatively small Poisson's ratio values (v = 0.18–0.20) are also consistent with relatively directional interatomic bonding and limited ductile response.

This mechanical softening is accompanied by a systematic reduction in Debye temperature from NaMgP to NaMgSb, which implies lower average phonon frequencies and enhanced phonon scattering (Snyder 2017). From a phonon-transport perspective, these characteristics favor reduced lattice thermal conductivity.

However, reduced lattice thermal conductivity alone does not guarantee superior thermoelectric performance, as the electronic transport parameters must also remain favorable (Chen et al., 2018; Rogl et al., 2016; Yongsheng, 2016).

The computed elastic constants for the lighter members of the series are broadly consistent with, but systematically softer than, values reported for the analogous Li-based half-Heuslers LiMgP and LiMgAs (Idrissi et al., 2023; Parsamehr et al., 2021), where the smaller ionic radius and stronger electronegativity of Li relative to Na produce a more compact lattice and correspondingly higher C11 and bulk modulus. This comparison supports the physical picture that Na substitution for Li in this family serves specifically to soften the lattice - a desirable feature for reducing lattice thermal conductivity - while the pnictogen substitution independently governs the electronic gap, so that the two design levers (A-site cation and pnictogen identity) act in a largely complementary rather than redundant manner across the wider AMgZ half-Heusler family.

Mechanical Stability and Elastic Behavior of NaMgZ

Table 2: Elastic Constants and Mechanical Properties of Namgz Compounds. Here, C_{11}, C_{12}, And C_{44} Are The Single-Crystal Elastic Constants, B Is The Bulk Modulus, G Is The Shear Modulus, E Is Young's Modulus (All In Gpa), N Is Poisson's Ratio (Dimensionless), And Θ_D Is The Debye Temperature (K)

Compound	*C*11	*C*12	*C*44	*B*	*G*	*E*	*v*	Θ_D
NaMgP	95.0	19.4	34.4	44.6	35.7	84.5	0.18	496.8
NaMgAs	79.8	17.3	30.5	38.1	30.8	72.8	0.18	374.8
NaMgSb	59.5	18.4	26.7	32.1	24.0	57.7	0.20	290.7

The band gaps obtained in this work agree closely with previously reported values for NaMgP and NaMgAs (NaMgP: 1.46 eV vs. 1.47 eV; NaMgAs: 0.88 eV vs. 0.83 eV; Arif et al., 2016), but show a larger discrepancy for NaMgSb (1.20 eV vs. 1.87 eV). This difference most likely reflects the well-documented tendency of GGA-PBE to systematically underestimate fundamental band gaps relative to gap-corrected approaches such as the Tran-Blaha modified Becke-Johnson potential or hybrid functionals; if the literature NaMgSb value was obtained using such a correction, or with a different pseudopotential/basis-set treatment of the Sb 5p states, part of the 0.67 eV difference is attributable to this well-known functional- and method-dependent effect rather than to an error in either calculation. We note this discrepancy explicitly here, rather than presenting the computed and literature values side by side without comment, and we recommend that a gap-corrected (e.g., TB-mBJ or GW) calculation for NaMgSb be pursued as a useful cross-check in future work.

Electronic Properties

The electronic properties of the NaMgZ (Z = P, As, Sb) compounds as shown in Figure 5, show clear trends that are important for thermoelectric applications. All materials exhibit well-defined band gaps, confirming their semiconducting nature. As seen in Table 1.

The band-gaps has direct implications for thermoelectric performance (Parsamehr et al; 2021). Intermediate gaps in NaMgAs and NaMgSb support a good balance between carrier excitation and Seebeck response, which is desirable for efficient thermoelectric transport, while the larger gap in NaMgP favors a stronger Seebeck response at the expense of requiring more aggressive carrier activation. Across the series, the moderate-to-large band gaps (0.88–1.46 eV) are large enough to suppress bipolar conduction at typical operating temperatures, which helps preserve thermopower (Snyder, 2017).

The projected density of states (PDOS) provides further insight into the origin of these electronic features. The states near the valence band maximum are mainly dominated by pnictogen p orbitals, while Na and Mg contribute mostly at deeper energy levels. This indicates that charge transport is primarily controlled by the pnictogen sublattice, with Na and Mg playing a supporting structural role. As a result, whole carriers are expected to dominate transport, consistent with p-type behavior.

The combination of band gap evolution and PDOS analysis shows that the NaMgZ compounds offer tunable electronic structures, where conductivity and thermopower can be balanced by controlling the pnictogen element (Snyder, 2017).

A closer inspection of the band curvature at the valence-band maximum and conduction-band minimum indicates a systematic trend in the effective masses across the series. In NaMgP, the valence band near the Fermi level is comparatively flat, consistent with a heavier hole effective mass and a correspondingly larger Seebeck

coefficient at a given carrier concentration. Moving toward NaMgAs and NaMgSb, the bands become progressively more dispersive, indicating lighter, more mobile carriers at the expense of some Seebeck response - the classic effective-mass/mobility trade-off in thermoelectric band engineering. A quantitative estimate of the valley degeneracy and band-edge effective masses via parabolic-band fitting or Boltzmann transport modeling is identified as a valuable next step beyond the scope of the present static electronic-structure analysis.

From a thermoelectric design perspective, the well-known heuristic that an optimal band gap for high-temperature operation lies roughly between six and ten times kBT (approximately 0.15-0.25 eV at 300 K, correspondingly larger at elevated operating temperatures) suggests that NaMgAs and NaMgSb, with gaps of 0.88 eV and 1.20 eV, are well positioned to suppress bipolar conduction across a wide operating-temperature window while retaining sufficient carrier activation at higher temperatures; NaMgP's larger 1.46 eV gap may require more aggressive doping or higher operating temperatures to activate a useful carrier density. Given that the projected density of states places the valence-band maximum predominantly on pnictogen p orbitals, acceptor-type extrinsic doping (for example, partial substitution of Mg by a lower-valence-electron-count element, or Na-site vacancies) is expected to be the more natural route to useful p-type carrier concentrations in this series, analogous to the doping strategies already established for p-type NbFeSb-family half-Heuslers. Benchmarked against the well-established ZrNiSn (n-type) and NbFeSb (p-type) half-Heusler thermoelectrics, which report room-temperature lattice thermal conductivities near 8-10 W/m/K and 3-4 W/m/K respectively and peak ZT values approaching or exceeding 1 after optimization (Quinn & Bos, 2021), the NaMgZ series offers a softer, more chemically tunable lattice - consistent with the lower Debye temperatures reported in Table 2 - that may be advantageous for further lattice-thermal-conductivity reduction, though at present the NaMgZ family has not yet been demonstrated experimentally and its electronic transport coefficients remain to be computed and validated against these established benchmarks.

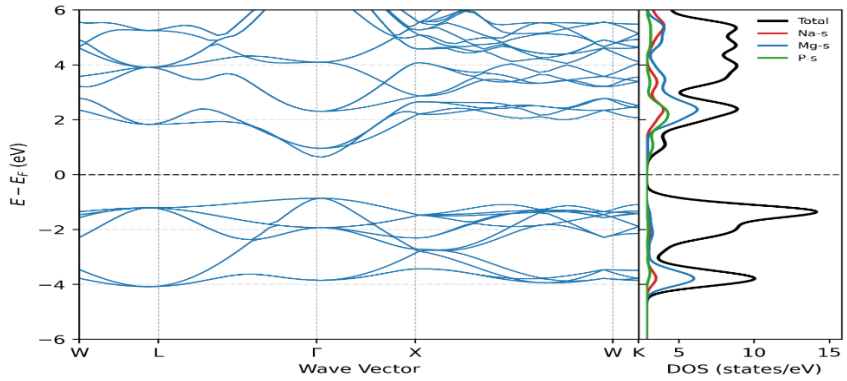

(a) NaMgP

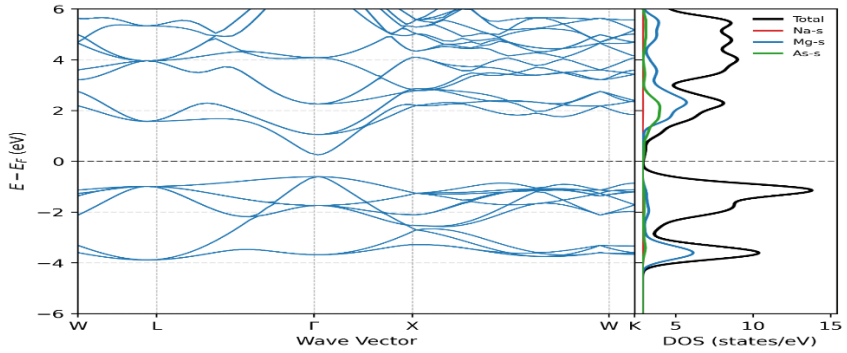

(a) NaMgAs

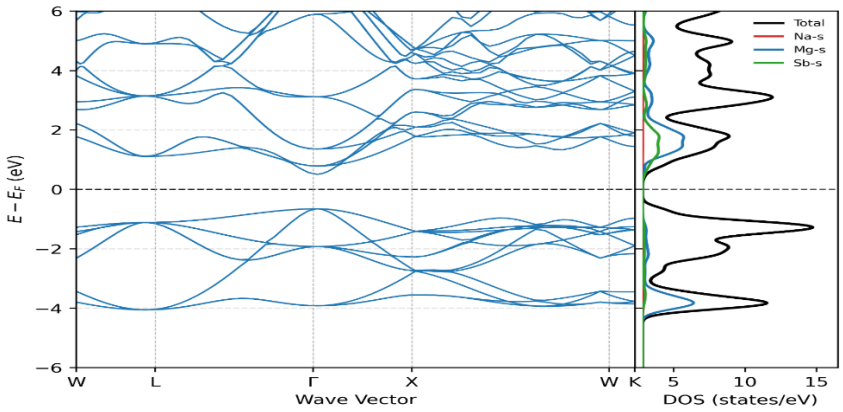

(b) NaMgSb

Figure 5: Electronic band structures and projected density of states (PDOS) of NaMgZ compounds: NaMgP, (b) NaMgAs and (c) NaMgSb

Several limitations of the present analysis should be stated explicitly. First, all reported band gaps are obtained at the GGA-PBE level, which is known to systematically underestimate fundamental gaps relative to experiment and relative to gap-corrected methods; the absolute gap values should therefore be interpreted primarily in terms of relative trends across the series rather than as quantitatively exact predictions. Second, all structural, elastic, and electronic properties reported here correspond to static, 0 K ground-state calculations and do not include finite-temperature effects such as thermal expansion or anharmonic phonon renormalization of the band gap. Third, the Debye temperature reported in Table 2 is used only as a qualitative proxy for relative lattice stiffness and phonon energy scale; it is not a substitute for an explicit phonon dispersion calculation or a Callaway/Boltzmann-transport estimate of the lattice thermal conductivity, neither of which was computed in this work. Finally, no explicit Seebeck coefficient, electrical conductivity, or power factor has been calculated; these quantities require semi-classical Boltzmann transport calculations (e.g., via BoltzTraP) built on top of the present band structures and are identified as the immediate priority for follow-up work.

CONCLUSION

In summary, the present first-principles investigation demonstrates that the NaMgZ (Z = P, As, Sb) half-Heusler series constitutes a chemically tunable platform for band-gap engineering with direct relevance to thermoelectric materials design. All three compounds retain the cubic half-Heusler phase and satisfy the expected criteria for thermodynamic and mechanical stability, confirming that pnictogen substitution does not destabilize the underlying framework. Across the series, the lattice constant increases systematically from NaMgP to NaMgSb, while the elastic moduli and Debye temperature decrease, indicating progressive lattice softening with increasing atomic mass of the pnictogen (Liu et al; 2025).

The electronic results reveal a clear and physically consistent evolution of the band structure. The band gap narrows from the lighter to the heavier compounds, reflecting changes in orbital hybridization, bonding strength, and relativistic effects. This trend is favorable from the perspective of carrier activation, but it also emphasizes the need to balance narrow-gap behavior against the increased likelihood of bipolar conduction, particularly in NaMgAs. When the structural, elastic, and electronic results are considered together, the intermediate members of the series appear to offer the most attractive compromise between semiconducting character, mechanical stability, and reduced phonon stiffness. Accordingly, NaMgAs and NaMgSb emerge as the most promising compositions for subsequent transport optimization, whereas NaMgP is likely to require stronger carrier activation.

This work establishes a coherent composition–property trend for NaMgZ compounds and shows that pnictogen substitution is an effective strategy for tuning the balance between electronic and lattice contributions relevant to thermoelectric performance. The results provide a strong foundation for future studies involving explicit transport coefficients, carrier doping, temperaturedependent phonon calculations, and experimental synthesis, and they support the view that rational band-gap engineering within the NaMgZ family can guide the development of improved half-Heusler-based thermoelectric materials. More broadly, given how comparatively unexplored Na-based half-Heuslers remain relative to their Li-based and

heavier-alkali counterparts, the present findings support extending this compositional strategy beyond the NaMgZ series to other Na-Mg-based and Na-substituted half-Heusler platforms as a potentially fruitful and currently underutilized route to new thermoelectric candidates.

REFERENCES

Anuradha, Kaur, K., Singh, R., & Kumar, R. (2018). Search for thermoelectricity in Li-based half-Heusler alloys: A DFT study. *Materials Research Express*, *5*, 014009. https://doi.org/10.1088/2053-1591/aaa507

Arif, M., Murtaza, G., Ali, R., Khenata, R., Takagiwa, Y., Muzammil, M., & Omran, S. B. (2016). Elastic and electro-optical properties of xyz compounds. *Indian Journal of Physics*, *90*(6), 639–647. https://doi.org/10.1007/s12648-015-0791-8

Blöchl, P. E. (1994). Projector augmented-wave method. *Physical Review B*, *50*(24), 17953–17979. https://doi.org/10.1103/PhysRevB.50.17953

Chen, Z., Zhang, X., & Pei, Y. (2018). Manipulation of phonon transport in thermoelectrics. *Advanced Materials*, *30*(17), 1705617. https://doi.org/10.1002/adma.201705617

Dal Corso, A. (2016). Elastic constants of beryllium: a first-principles investigation. *Journal of Physics: Condensed Matter*, *28*(7), 075401. https://doi.org/10.1088/0953-8984/28/7/075401

Giannozzi, P., Andreussi, O., Brumme, T., Bunau, O., Buongiorno Nardelli, M., Calandra, M., & Baroni, S. (2017). Advanced capabilities for materials modelling with Quantum ESPRESSO. *Journal of physics: Condensed matter*, *29*(46), 465901. https://doi.org/10.1088/1361-648X/aa8f79

Giannozzi, P., Baseggio, O., Bonfà, P., Brunato, D., Car, R., Carnimeo, I., & Baroni, S. (2020). Quantum ESPRESSO toward the exascale. *The Journal of chemical physics*, *152*(15), 154105. https://doi.org/10.1063/5.0005082

Huang, L., Zhang, Q., Yuan, B., Lai, X., Yan, X., & Ren, Z. (2016). Recent progress in half-Heusler thermoelectric materials. *Materials Research Bulletin*, *76*, 107–112. https://doi.org/10.1016/j.materresbull.2015.11.032

Husain, M., Albalawi, H., Al Huwayz, M., Khan, R., & Rahman, N. (2023). First-principle computation of some physical properties of half-Heusler compounds for possible thermoelectric applications. *RSC Advances*, *13*(34), 23716–23727. https://doi.org/10.1039/D3RA04192A

Idrissi, S., Labrim, H., & Bahmad, L. (2023). Study of structural, electronic and optoelectronic properties of the half-heusler limgz (z = n, p or sb) materials: Dft and tddft approaches. *Ferroelectrics*, *615*(1), 241–255. https://doi.org/10.1080/00150193.2023.2171461

Jaishi, Dhurba & Sharma, Nileema & Karki, Bishnu & Belbase, Bishnu & Adhikari, Rajendra & Ghimire, Madhav. (2021). Electronic structure and thermoelectric properties of half-Heusler alloys NiTZ. AIP Advances. 11. 025304. https://doi.org/10.1063/5.0031512.

M. Born, On the stability of crystal lattices. i, in: Mathematical Proceedings of the Cambridge Philosophical Society, Vol. 36, Cambridge University Press, 1940, pp. 160–172. https://doi.org/10.1017/S0305004100017138

Miao, L., Zhu, S., Liu, C., Gao, J., Zhang, Z., Peng, Y., & Mori, T. (2024). Comfortable wearable thermoelectric generator with high output power. *Nature Communications*, *15*(1), 8516. https://doi.org/10.1038/s41467-024-52841-1

Monkhorst, H., & Pack, J. (1976). Special points for brillouin-zone integrations. *Phys. Rev. B*, *13*, 5188–5192. https://doi.org/10.1103/PhysRevB.13.5188

Perdew, J. P., Burke, K., & Ernzerhof, M. (1996). Generalized gradient approximation made simple. *Physical Review Letters*, *77*, 3865–3868. https://doi.org/10.1103/PhysRevLett.77.3865

Quinn, R. J., & Bos, J.-W. G. (2021). Advances in half-heusler alloys for thermoelectric power generation. *Materials Advances*, *2*(19), 6246–6266. https://doi.org/10.1039/D1MA00707F

Rogl, G., Grytsiv, A., Gürth, M., Tavassoli, A., Ebner, C., Wünschek, A., Puchegger, S., Soprunyuk, V., Schranz, W., Bauer, E., Müller, H., Zehetbauer, M., & Rogl, P. (2016). Mechanical properties of half-Heusler alloys. *Acta Materialia*, *107*, 178–195. https://doi.org/10.1016/j.actamat.2016.01.031

S. Liu, W.-D. Liu, W. Lyu, L.-C. Yin, Y. Yue, H. Gao, M. Li, X.-L. Shi, Q. Liu, N. Wang, J. D. Riches, D. V.

Golberg, Z.-G. Chen, Alignment of edge dislocations: the reason lying behind composition inhomogeneity induced low thermal conductivity, Nature Communications 16 (2025) 1–12. https://doi.org/10.1038/s41467-025-64749-5

S. Parsamehr, A. Boochani, M. Amiri, S. Solaymani, E. Sartipi, S. Naderi, A. Aminian, Thermodynamic phase diagram and thermoelectric properties of limgz (z = p, as, bi): ab initio method study, Philosophical Magazine 101 (3) (2021) 369–386. https://doi.org/10.1080/14786435.2020.1839138

Snyder, G. J., & Snyder, A. H. (2017). Figure of merit ZT of a thermoelectric device defined from materials properties. *Energy & environmental science*, *10*(11), 2280-2283. https://doi.org/10.1039/C7EE02007D

Yadav, M. K., & Sanyal, B. (2015). First principles study of thermoelectric properties of li-based half-heusler alloys. *Journal of Alloys and Compounds*, *622*, 388–393. https://doi.org/10. 1016/j.jallcom.2014.10.027

Yongsheng, Z. (2016). First-principles debye–callaway approach to lattice thermal conductivity. *Journal of Materiomics*, *2*, 237–247. https://doi.org/10.1016/j.jmat.2016.08.005

Zhao, H., Cao, B., Li, S., Liu, N., Shen, J., Li, S., Jian, J., Gu, L., Pei, Y., Snyder, G. J., Ren, Z., & Chen, X. (2017). Engineering the thermoelectric transport in half-Heusler materials through a bottom-up nanostructure synthesis. *Advanced Energy Materials*, *7*(18), 1700446. https://doi.org/10.1002/aenm.201700446